Influence of target–substrate angle on the elemental concentration of c-axis YBa 2 Cu 3 O 7−x thin films

D. E. Pugel and L. H. Greene

Citation: Applied Physics Letters **75**, 1589 (1999); doi: 10.1063/1.124763
View online: http://dx.doi.org/10.1063/1.124763
View Table of Contents: http://scitation.aip.org/content/aip/journal/apl/75/11?ver=pdfcov
Published by the AIP Publishing

Influence of target–substrate angle on the elemental concentration of *c*-axis $YBa_2Cu_3O_{7-x}$ thin films

D. E. Pugel and L. H. Greene[a)]
Department of Physics and Materials Research Laboratory, University of Illinois Urbana-Champaign, Urbana, Illinois 61801

(Received 26 May 1999; accepted for publication 20 July 1999)

The thermalization processes in sputtering suggest a spatial dependence of elemental concentration in the sputter plume. A variety of analysis techniques demonstrate that *c*-axis films grown at angles which deviate from the standard off-axis geometry produce nominally $YBa_2Cu_3O_{7-x}$ in the bulk with dramatic changes in the surface morphology and deposition rate. In addition to the common materials characterization techniques of scanning electron microscopy, x-ray diffraction, transport measurements, and conventional Rutherford backscattering spectrometry (RBS), angle-dependent RBS is employed to probe surface inhomogeneities of films grown at target–substrate angles away from the standard off-axis position. © *1999 American Institute of Physics.* [S0003-6951(99)02237-8]

Understanding the growth of epitaxial thin films of $YBa_2Cu_3O_{7-x}$ (YBCO) is essential for the fabrication of devices suitable for scientific investigation and technical applications. Ongoing studies of the growth conditions for high T_c thin films elucidate the conditions which minimize surface roughness,[1] describe surface inhomogeneities, and uncover the nature of the growth mechanism itself. dc magnetron sputtering has emerged as an accepted method for the growth of high-quality superconducting thin films due to the extent of epitaxy and capacity to produce smooth surfaces.[2,3] In the off-axis sputtering configuration, a single stoichiometric ceramic target yields on-stoichiometric superconducting films.[4] Away from the standard off-axis position, energy distributions of sputtered elements vary spatially within the sputter plume as a consequence of the angular dependence of thermalization.[5–7] Variations in the sputter plume alter the cation concentration at the substrate and therefore promote mixed growth of *a*-, *b*- and *c*-axis grains, surface oxides, and modify bulk stoichiometry in the film. The potential for such detrimental effects altering film quality only increases with deviations from 90° off-axis growth, hence, with increasing film area. To study the effect of these differences in cation concentration in the sputter plume, we have grown thin films of *c*-axis oriented YBCO using off-axis sputter deposition with the target tilted at varying angles from the standard 90° off-axis position.

Rutherford backscattering spectrometry (RBS), a commonly used method for stoichiometric determination of high T_c films, is a noninvasive method with elemental sensitivity.[8] We show that angle-dependent RBS is a powerful tool to uncover the film thickness and elemental concentration of dense surface structures.[9]

In this letter, combined results from RBS, scanning electron microscopy, x-ray diffraction, and four-probe transport measurements reveal that differences in elemental concentration due to variation in growth angle do not modify bulk film stoichiometry, but produce oxide precipitates on the surface. Changes in the deposition rate also emerge.

c-axis films are deposited by dc magnetron sputtering from a commercial on-stoichiometric ceramic target in an atmosphere of $Ar:O_2$ (4:1) at 170 mTorr. The growth temperature is stabilized at 735 °C after 2 h of presputtering. The sputter target is held at a fixed angle for the duration of growth. The angle of deviation from the standard off-axis position is defined as the *target–substrate angle*, ϕ. At $\phi = 0°$, the face of the target and substrate surfaces are at 90° with respect to each other. Positive (negative) ϕ indicates the target is tilted away from (toward) the substrate plane, resulting in a sputter angle greater than (less than) the standard 90° off-axis direction. All film growth occurs in the near-off-axis regime, at high oxygen pressures and with a target that is not highly oxygenated, rendering resputtering effects insignificant.[10]

A Van der Graaff accelerator with 2.0 meV $^4He^+$ ions at a beam current of 10 nA and spot diameter of 2 mm is employed in the RBS study. The beam current is measured with a Faraday cup after each run. Alpha particles backscatter onto a silicon surface barrier detector positioned at 165°, with a resolution of 15.1 keV at FWHM. Samples are mounted onto a two-axis goniometer. Using a laser beam collinear with the particle beam, the sample is aligned with the detector by viewing the sample-reflected beam position relative to the detector aperture. The estimated error is ±0.5°. All RBS spectra are analyzed with RUMP analysis software[11,12] using appropriate correction factors.

Figure 1 displays scanning electron micrographs (SEMs) of films deposited at six target-to-substrate angles. The standard *c*-axis growth geometry, $\phi = 0°$, produces a typical *c*-axis surface: A few ''stones'' (oxide precipitate) and deep rivulets are seen on an otherwise smooth surface. Away from $\phi = 0°$, there exist two different growth morphologies: ball-like structures, or ''stones'' and block-like structures or ''sticks.'' The stones appear at small $|\phi|$ and are about 0.6 μm in diameter. Sticks appear at large $|\phi|$, with increasing density at, and above, $|\phi| = 10°$. They ap-

a)Electronic mail: lhg@uiuc.edu

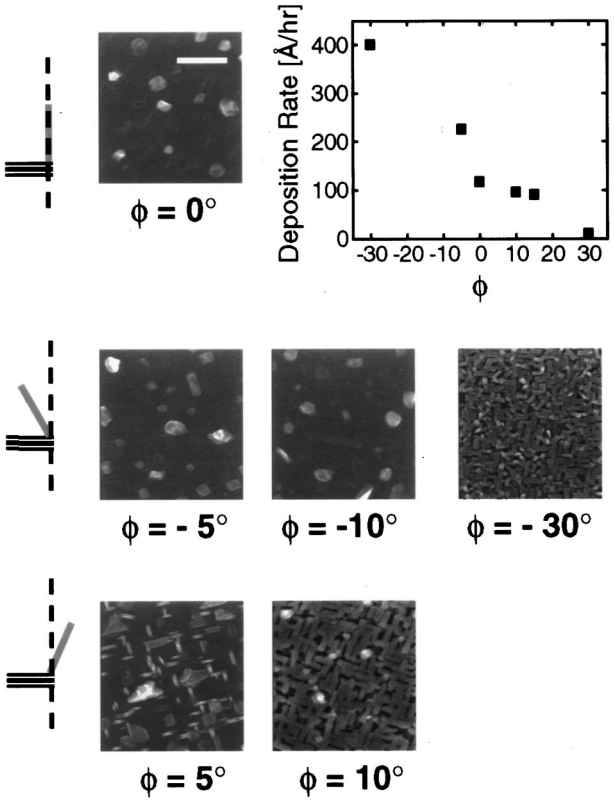

FIG. 1. Scanning electron micrographs of films grown at various target-to-substrate angles ϕ. The bar in the upper right hand corner of the $\phi=0°$ micrograph represents 1.5 μm. Samples are grown on (100) $SrTiO_3$ substrates affixed to a substrate heater using conductive silver ink. The surface morphology is symmetric in ϕ, with block-like structures. The upper-right corner shows the deposition rate as a function of target–substrate angle, ϕ. The rate decreases with positive target-to-substrate angle away from the off-axis position rate. This can be understood as a decreased flux of sputtered elements in the immediate vicinity of the substrates.

pear to rest horizontally on the surface, reminiscent of *a*-axis growth, and increase in density and in surface area with increasing $|\phi|$. At $\phi=-30°$, the average length of a stick is 0.5 μm. The angular variation in surface morphology is nominally symmetric in both tilt directions, with a gradual increase in block structures with increasing $|\phi|$.

The composition of these surface structures is determined using RBS. Figure 2 shows a striking difference in the

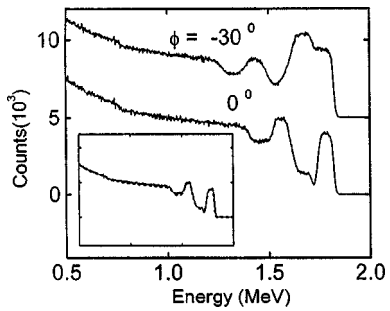

FIG. 2. Comparison of RBS spectra for $\phi=-30°$ (upper curve) and $\phi=0°$ (lower curve) films. The upper curve is offset by 4000 counts for clarity. There is a large shift in the positions of the low-energy edges of the elemental peaks in $\phi=-30°$ relative to the $\phi=0°$ film, indicating a larger film thickness, consistent with increased (decreased) deposition rates with negative (positive) ϕ. In the inset is the same $\phi=0°$ film data, fit using RUMP simulation (dotted line) with a substrate thickness of 200 000 Å. A Bohr straggling factor of 10 is applied to the simulation data to account for energy loss in Sr and Ti.

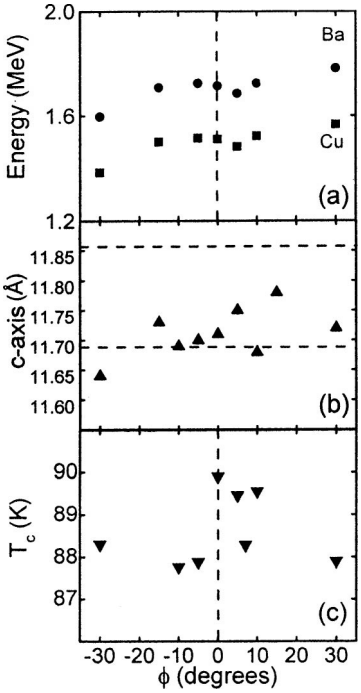

FIG. 3. (a) Shift of RBS peak positions as a function of target-to-substrate angle ϕ. Shift of peak positions is proportional to the film thickness. Yttrium edges were not resolvable due to superposition of the Sr substrate edges over the Y peaks. (b) and (c) *c*-axis length and T_c, respectively, as a function of ϕ. Neither *c*-axis length nor T_c show angular dependence and lie within reasonable error of accepted values, indicating minimal change in the bulk properties of the films.

positions of the low-energy edges of films grown at $\phi=0°$ and $-30°$. In the inset, the $\phi=0°$ data are fit to a RUMP simulation where layer 1 is $YBa_2Cu_3O_7$ of a thickness 1200 Å and layer 2 is the $SrTiO_3$ substrate. In Fig. 3(a), films grown at negative ϕ exhibit a shift to lower energies for the left edges of the peak. This shift in the low-energy edge with increasing $|\phi|$ is a consequence of backscattering events through dense stick structures at the surface and increased film thickness. Normalizing film thickness over deposition times demonstrates increasing deposition rate with decreasing ϕ (see upper right of Fig. 1).

The effect of increased elemental concentration and film thickness on the superconducting and structural properties of the YBCO films are investigated with four-probe resistivity versus temperature and x-ray diffraction measurements, respectively [Figs. 3(b), 3(c)]. The superconducting transition temperature T_c is 89 ± 3 K for every film. The *c*-axis lattice spacing, derived from the (005) Bragg reflection, is 11.7 ± 0.07 Å, independent of ϕ. These *c*-axis lengths fall within the published range for ''optimally doped'' YBCO thin films.[13] Scans in the Bragg–Bretano geometry (θ–2θ reflection) reveal *c*-axis oriented films, with additional phases present in films grown at larger $|\phi|$.

Combining bulk measurement results with RBS and SEM, we determine that films grown away from the off-axis position develop dense surface precipitates, thereby increasing surface roughness. This is verified by RBS spectrometry performed at different incident angles.[14,15] Path lengths of α particles at different incident angles will differ, probing more or less surface material, altering peak positions. The change in yield is proportional to the cosine of the incident angle.[16]

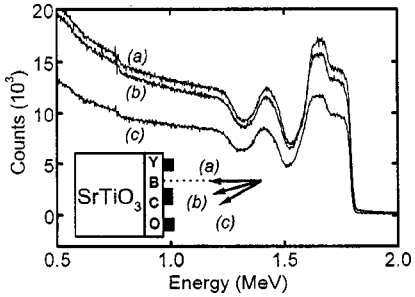

FIG. 4. RBS spectrum of $\phi=-30°$ film for three $^4He^+$ ion incident angles relative to the sample normal. Curve (a) is at near-normal (5°) incidence, curve (b) is the standard incidence relative to surface normal angle (30°), and curve (c) is near-grazing incidence. A longer path traversed by the α particles, due to a shallow incidence, leads to increased interactions between α particles and the electronic structure of the precipitate, reducing backscattered energy. As the goniometer approaches the sample normal, the path length through the surface oxides is shorter, reducing the yield and shifting both low and high-energy edges to the left as seen in curve (a).

Figure 4 demonstrates that for the $\phi=-30°$ film at grazing incidence, the thickness of the oxide layer exaggerates widths and yield, as in curve (c). At angles closer to the surface normal, less of the precipitate is probed, decreasing the peak width as well as the yield, as seen in curves (b) and (c). Roughness rounds off the high-energy edges of the peaks due to an averaging of multiple path lengths traversed by the α particles in the precipitate.

The films with $\phi\neq0°$ are modeled as a trilayer of oxide precipitates (Y_2O_3 and $BaCuO_2$), on-stoichiometric YBCO and the $SrTiO_3$ substrate, as seen in Fig. 5. There is an excellent fit between the simulated trilayer and measured film. The additional phases at the surface are expected due to the departure from stoichiometric deposition conditions in the sputter plume. Typical phases in equilibrium with YBCO include: Y_2BaCuO_5, CuO, Y_2O_3, and $BaCuO_2$.[17] The existence of this precipitate is confirmed by x-ray diffraction data (inset to Fig. 5) which show three additional peaks in the $\phi=-30°$ spectrum, corresponding to the oxides Y_2O_3 and $BaCuO_2$.[18,19]

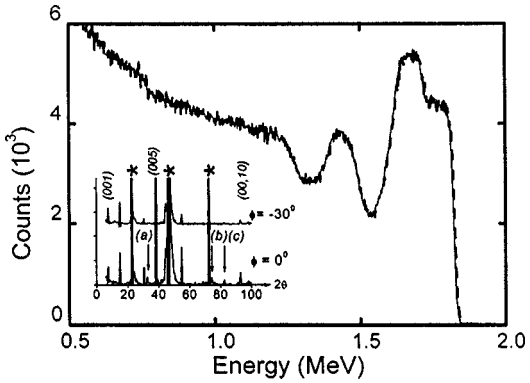

FIG. 5. RBS spectrum of $\phi=-30°$ film (solid line) with a RUMP fit of a trilayered film to include the presence of surface precipitates (dotted line). The trilayer consists of a top (precipitate) layer of $Y_{1.75}Ba_{0.75}Cu_{0.75}O_5$ 3500 Å thick, a middle layer of $YBa_2Cu_3O_7$ 750 Å thick, and a bottom layer of $SrTiO_3$ 200 000 Å thick. The precipitate layer can be stoichiometrically reduced to two common surface oxides: Y_2O_3 and $BaCuO_2$. The inset is a comparison of the x-ray diffraction data for the $\phi=-30°$ (lower curve) and $\phi=0°$ (upper curve). The (001), (005), and (00,10) Bragg reflections of YBCO are labeled with respective Miller indices. $SrTiO_3$ substrate peaks superposed with (003), (006) and (009) YBCO peaks are marked with an asterisk (*). Consecutive reflections of YBCO peaks between (001) and (00,10) are the remaining unmarked peaks. (a), (b), and (c) correspond to the oxides Y_2O_3 and $BaCuO_2$ (Refs. 18 and 19). Rocking curves for all films are ~0.03° FWHM, indicating well-textured films.

Through the use of an array of bulk and surface characterization techniques, we have illustrated that variations in ϕ, the target-to-substrate angle in dc magnetron sputtering, lead to modifications in elemental concentration and deposition rate. This increase in elemental concentration leads to a surface precipitate and increased overall thickness of the film as evidenced by measurements by RBS, XRD, and SEM. Bulk measurements demonstrate that the film remains nominally $YBa_2Cu_3O_{7-x}$.

This work is supported by the NSF Science and Technology Center for Superconductivity (Grant No. NSF-DMR91-20000) and GAANN Fellowship, U.S. Department of Education. All materials characterization was performed at the Center for Microanalysis of Materials, University of Illinois, Urbana-Champaign (Grant No. DOE-DEFG02-91-ER45439). The authors acknowledge technical assistance from W. L. Feldmann, B. Clymer, M. Sardela, and seminal discussions with B. G. Bagley.

[1] B. Wuyts, Z. X. Gao, M. Maenhoudt, E. Osquiguil, and Y. Brunynseraede, Physica C **203**, 235 (1992).
[2] C. B. Eom, J. Z. Sun, K. Yamamoto, A. F. Marshall, K. E. Luther, T. H. Geballe, and S. S. Laderman, Appl. Phys. Lett. **55**, 595 (1989).
[3] R. L. Sandstrom, W. J. Gallagher, T. R. Dinger, R. H. Koch, R. B. Laibowitz, A. W. Kleinsasser, R. J. Gambino, B. Bumble, and M. F. Chisholm, Appl. Phys. Lett. **53**, 444 (1988).
[4] B. G. Bagley, L. H. Greene, P. Barboux, J. M. Tarascon, T. Venkatesan, E. W. Chase, Siu-Wai Chan, W. L. Feldmann, B. J. Wilkins, S. A. Khan, and M. Giroud, in *Advances in Superconductivity I*, edited by K. Kitazawa (Springer, Tokyo, 1989), p. 478.
[5] K. Meyer, I. K. Schuller, and C. M. Falco, J. Appl. Phys. **52**, 5803 (1981).
[6] J. A. Valles-Abarca and A. Gras-Marti, J. Appl. Phys. **55**, 1370 (1984).
[7] G. Betz and G. K. Wehner, in *Sputtering By Particle Bombardment II*, edited by R. Behrisch (Springer, Berlin, 1983), p. 11.
[8] W. K. Chu, J. W. Mayer, and M-A. Nicolet, *Backscattering Spectrometry* (Academic, New York, 1978).
[9] J. S. Williams, Nucl. Instrum. Methods **149**, 207 (1978).
[10] M. Migliuolo, R. M. Belan, and J. A. Brewer, Appl. Phys. Lett. **56**, 2572 (1990).
[11] J. C. Cheang Wong, J. Li, C. Ortega, J. Siejka, G. Vizkelethy, and Y. Lemaitre, Nucl. Instrum. Methods Phys. Res. B **64**, 169 (1992).
[12] O. Bøgensen and D. A. Lillenfeld, Nucl. Instrum. Methods Phys. Res. B **36**, 1 (1989).
[13] C. B. Eom, J. Z. Sun, B. M. Lairson, S. K. Streiffer, A. F. Marshall, K. Yamamoto, S. M. Anlage, J. C. Brauman, T. H. Geballe, S. S. Laderman, R. C. Taber, and R. D. Jacowitz, Physica C **171**, 354 (1990).
[14] K. Schmid and H. Ryssel, Nucl. Instrum. Methods **119**, 287 (1974).
[15] A. R. Knudson, Nucl. Instrum. Methods **168**, 163 (1980).
[16] R. D. Edge and U. Bill, Nucl. Instrum. Methods **168**, 157 (1980).
[17] R. Beyers and B. T. Ahm, Annu. Rev. Mater. Sci. **21**, 335 (1991).
[18] D. Grier and G. McCarthy, North Dakota State University, Fargo, North Dakota, ICDD Grant-in-Aid JCPDS: 43-1036 (1991).
[19] W. Wong-Ng, H. McMurdie, B. Paretzkin, C. Hubbard, and A. Dragoo, NBS, Gaithersburg, MD, ICDD Grant-In-Aid JCPDS: 38-1402 (1991).